Proceedings of the 4th International Conference on Functional Materials and Civil Engineering
DOI: 10.54254/2755-2721/2026.36832

Graphene-Based Materials for Energy Storage Applications in Zinc Ion Batteries

Sizhen Wu*, Xinmiao Gan

College of Chemistry and Molecular Science, Anhui Normal University, Wu'hu, China
**Corresponding Author. Email: wusizhen@ahnu.edu.cn*

Abstract. Zinc offers clear advantages—affordability, safety, and high capacity—that have fueled research into aqueous ZIBs as a potential successor to lithium batteries. Despite this potential, multiple intertwined issues persist: dendrite formation cannot be reliably suppressed, side reactions plague the interfaces, cathode structures tend to degrade or release active components, and the aqueous electrolyte itself suffers from a limited stable potential range. Collectively, these challenges impede practical deployment. Graphene-based materials (GBs) offer a flexible materials platform for mitigating these problems: their conductive skeletons accelerate charge transfer, their surface chemistry can regulate interfaces, and their mechanical and chemical robustness helps protect unstable components. This review first analyzes the principal failure mechanisms of ZIBs and then summarizes the roles of GBs in cathodes, anodes, electrolytes, separators, and current collectors. Remaining bottlenecks and design priorities for scalable, long-life GB-assisted ZIBs are also discussed.

Keywords: Zinc ion batteries, Graphene-based materials, Anode, Cathode, Electrolyte, Separator

1. Introduction

A pressing demand has emerged for cost-effective, high-efficiency, and eco-friendly energy storage systems, driven by the worldwide push toward low-carbon power networks.

Lithium-ion batteries remain dominant, but resource uncertainty, cost pressure, safety concerns, and environmental burdens weaken their suitability for large-scale grid storage and some portable applications [1-3]. ZIBs have therefore attracted broad interest because metallic zinc is abundant, inexpensive, relatively benign, has a high theoretical gravimetric capacity, and operates at a favorable redox potential (Figure 1) [4-7]. The drop in Coulombic efficiency and the notable reduction in operational durability arise directly from dendrite formation, hydrogen release, corrosive reactions, and surface passivation at the zinc electrode. On the cathode side, active-species dissolution, lattice strain during ion storage, and low electronic conductivity limit both durability and energy output. The cyclability and upscaling potential are further constrained by the restricted operational window of the aqueous electrolyte, the limited mechanical/chemical durability and elevated cost of separators, as well as the corrosion-induced or dendrite-initiated degradation of current collectors [8-11].

© 2026 The Authors. This is an open access article distributed under the terms of the Creative Commons Attribution License 4.0 (https://creativecommons.org/licenses/by/4.0/).

DOI: 10.54254/2755-2721/2026.36832

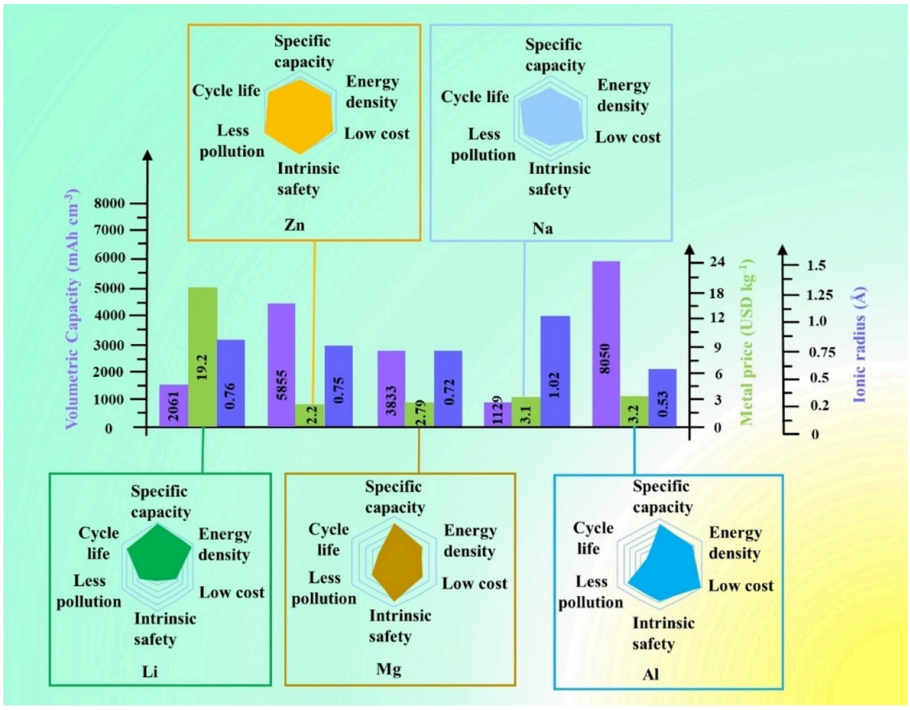

Figure 1. Comparison of typical Li, Zn, Mg, Na and Al metal anodes in terms of capacity, metal price and ionic radius, as well as comparison of their specific capacity, cycle life, low pollution, low cost, intrinsic safety, and energy efficiency radar plots [12]

Since the isolation of atomically thin carbon films in 2004 [13], Considerable interest has been directed toward graphene and its derivatives, driven by their large accessible surface area, superior charge-transport capability, outstanding mechanical performance, and high chemical stability [13-16]. When incorporated into ZIBs, GBs can redistribute current, facilitate ion transport, inhibit dendrite propagation, and reinforce unstable electrode structures [12].

This review summarizes the main challenges of ZIBs, the properties that make GBs useful in this system, recent applications in key battery components, and future directions for practical cell design.

2. Challenges in zinc-ion batteries

Although aqueous ZIBs have developed rapidly, practical grid and portable devices are still limited by several interacting failure modes:

(1) Cathode instability. Dissolution of active species, electrode volume variation, and framework collapse can occur during repeated Zn^{2+} insertion and extraction [17].

(2) Anode irreversibility. Collective impairments from dendritic nucleation, hydrogen side reactions, chemical corrosion, and surface blocking (passivation) lead to poor Zn utilization and diminished Coulombic reversibility [18].

(3) Electrolyte constraints. Free water and the limited electrochemical stability window accelerate parasitic reactions and restrict operating voltage [9, 19].

(4) Separator deficiencies. Thick separators lower energy density, whereas uneven pore structures encourage nonuniform ion flux and dendrite penetration [20].

(5) Current collector limitations. Metallic collectors can suffer from corrosion, insufficient interfacial stability, and limited mechanical tolerance under repeated cycling [21].

DOI: 10.54254/2755-2721/2026.36832

3. Performance of graphene-based materials

The atomically thin honeycomb lattice of graphene gives GBs a combination of transport, surface, and mechanical properties that is particularly relevant to ZIB design.

A large accessible surface area supplies abundant pores, defects, and edge sites, which shortens ion-diffusion pathways and increases the electrochemically active interface [22, 23]. In three-dimensional porous frameworks, GBs also dilute the local current density on zinc anodes, promote more homogeneous nucleation, and slow dendrite growth, thereby improving cycling stability and Coulombic efficiency [24].

Many ZIB cathodes are semiconducting or nearly insulating [12, 25]. Graphene can bridge active particles into a continuous electron pathway: its high carrier mobility supports fast electron transport, while its lamellar morphology creates line or face contacts with the host material [26]. As a result, sluggish transport through poorly conductive phases is replaced by charge movement along a conductive scaffold, improving reaction kinetics and rate performance [27].

The high Young's modulus, tensile strength, and flexibility of GBs also help electrodes tolerate mechanical stress [28]. In artificial interphases or composite zinc hosts, graphene-rich layers restrain dendritic protrusions and favor lateral zinc deposition [29]. In cathodes, graphene additives or frameworks accommodate repeated insertion/extraction strain, reducing pulverization, particle detachment, and loss of electrical contact [30].

Mechanical design can slow physical damage, but chemical degradation requires materials that remain stable in aqueous environments [31]. GBs are comparatively inert and corrosion-resistant; they do not readily dissolve in electrolyte or catalyze water splitting [32, 33]. On zinc anodes, they can suppress corrosion and hydrogen evolution [33, 34]. Around cathode particles, a three-dimensional graphene network can act as a chemical and physical barrier that limits dissolution and structural collapse [32, 35].

4. Applications of graphene-based materials in key components of zinc-ion batteries

4.1. Cathode

Cathode research commonly combines GBs with manganese compounds, vanadium compounds, organic electrodes, and Prussian blue analogues. Across these families, graphene is mainly introduced to build conductive pathways, stabilize the host framework, regulate ion transport, or protect active phases. MOF-derived, MXene-containing, and other hybrid systems have also been reported, but their graphene-related functions largely overlap with the mechanisms discussed below.

4.1.1. Manganese-based materials

Manganese oxides, particularly the α-, β-, and γ-polymorphs, exhibit tunnel or layered host structures [36, 37]. In the layered derivatives, the incorporation of interlayer water serves to screen the high Coulombic repulsion of Zn^{2+} species and concurrently diminishes the energy barriers for intercalation/deintercalation. These cathodes exhibit a relatively flat discharge plateau at ~1.2–1.4 V (vs. Zn^{2+}/Zn) and a high theoretical specific capacity of 616 mAh g^{-1}, which are attributed to the Mn^{4+}/Mn^{2+} redox couple, thereby making them strong contenders for aqueous ZIBs [38, 39]. Nonetheless, their further advancement is hindered by deficient electronic conductivity, excessive polarization at high rates, and dissolution issues originating from Mn^{3+} disproportionation—factors that accelerate lattice collapse and precipitate irreversible capacity fading [38, 40].

DOI: 10.54254/2755-2721/2026.36832

Li and co-workers integrated alpha-MnO_2 with graphene by a microwave-hydrothermal route, producing a three-dimensional conductive framework and increasing the pseudocapacitive contribution to 34%. The Mn^{4+}/Mn^{2+} redox reaction endows these cathodes with a stable voltage output of approximately 1.2–1.4 V (vs. Zn^{2+}/Zn) and an impressive theoretical capacity of 616 mAh g^{-1}, qualities that underscore their potential in aqueous zinc-ion battery systems (Figure 2a) [41]. By wrapping oxygen-deficient β-MnO_2 nanorods with GO, Ding et al. introduced Mn–O–C bonds that cut the bandgap down to 0.12 eV and mitigated Mn dissolution; this electrode subsequently attained 236.6 mAh g^{-1} at 1 C, with proton intercalation prevailing over Zn^{2+} storage (Figure 2b) [42]. In the case of γ-MnO_2, a cathode design achieved 361.8 mAh g^{-1} at 0.5 A g^{-1} and exhibited 94 % capacity maintenance after 700 cycles. Such outstanding results are attributable to the synergistic insertion of both H^+ and Zn^{2+}(Figure 2c) [43].

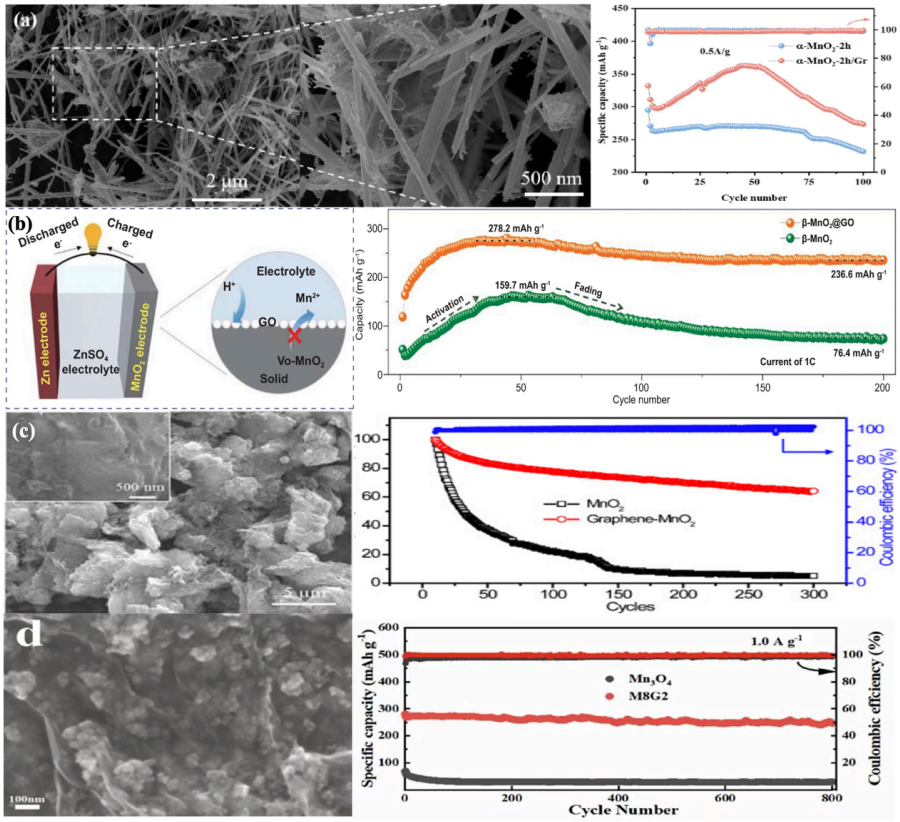

Figure 2. (a) α-MnO_2-2h/Gr SEM images and α-MnO_2-2h/Gr and α-MnO_2-2 h Cycling performance at 0.5 A g^{-1} [41], (b) Working schematic diagram of the Zn//β-MnO_2@GO battery and Cycling performances of β-MnO_2 and β-MnO_2@GO electrodes at the rate currents of 1C [42], (c) SEM images of MnO_2-graphene sample and cycling performance for the MnO_2 and MnO_2-graphene electrodes, as well as the corresponding Coulombic efficiency for the Zn//MnO_2-graphene battery [43], (d) SEM images of M8G2 and cycling stability curves and Coulombic efficiency of Mn_3O_4 and M8G2 electrodes at 1A g^{-1} [44]

Employing a room-temperature oxidation–reduction strategy, Yang et al. constructed a Mn_3O_4-rGO composite whose interconnected rGO skeleton not only prevented particle agglomeration but also alleviated volume expansion. At a current density of 0.1 A g^{-1}, the M8G2 electrode yielded 522.3 mAh g^{-1}, nearly triple the value of pristine Mn_3O_4 (199.5 mAh g^{-1}). Furthermore, it preserved

DOI: 10.54254/2755-2721/2026.36832

89.3 % of its capacity over 800 cycles, with the dual-ion (H^+/Zn^{2+}) co-insertion mechanism responsible for these enhancements (Figure 2d) [44].

4.1.2. Vanadium-based materials

Vanadium-based cathodes can deliver high theoretical capacities, commonly in the 200-400 mAh g^{-1} range, because vanadium supports multiple redox states from V^{2+} to V^{5+} [45, 46]. Their layered or open-tunnel frameworks can accommodate Zn^{2+} insertion and reduce lattice strain, and structural water may act as a pillar that screens Zn^{2+} charge and lowers diffusion barriers [45-49]. Their operating potentials are compatible with zinc anodes [46, 50] and strategies such as pre-intercalation, oxygen-vacancy engineering, and carbon compositing further improve stability [51, 52]. Even so, vanadium dissolution and phase-transition-related fading remain major obstacles [46, 50].

Muthukumar et al. prepared V_2O_5 nanobelt/rGO hybrids by microwave-assisted exfoliation followed by Zn^{2+}/Mn^{2+} coprecipitation. Mn ions appear to act as more stable interlayer pillars, as evidenced by the following comparison: the Zn^{2+}-only sample gave 395 mAh g^{-1} at 0.5 A g^{-1} but lost 72 % of its capacity over 2000 cycles, while the Zn^{2+}/Mn^{2+} co-intercalated material delivered 291 mAh g^{-1} at 4 A g^{-1} and preserved 77 % after the same number of cycles (Figrue 3a) [53].

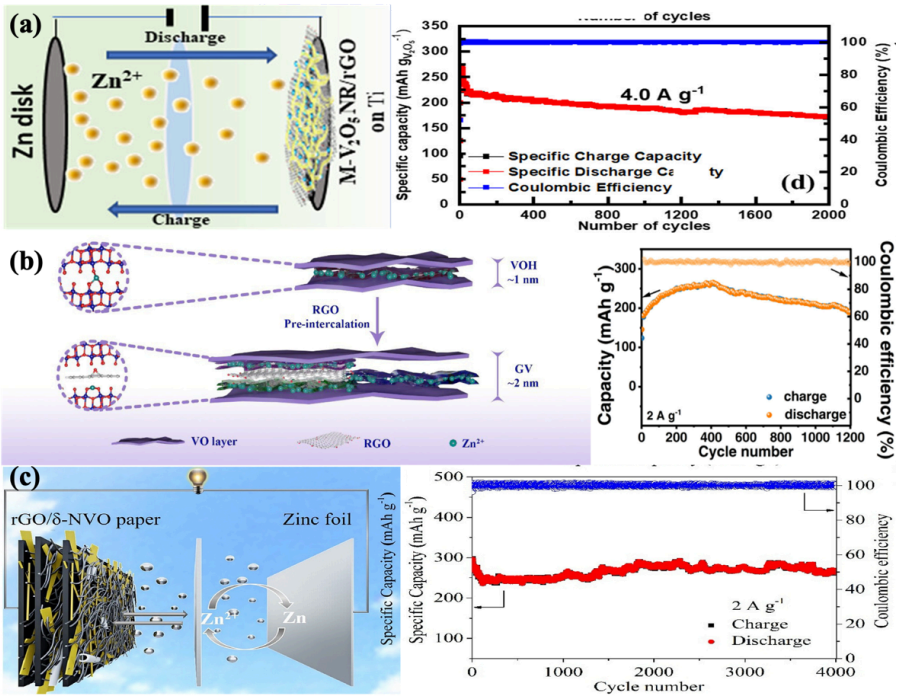

Figure 3. (a) Working schematic diagram of the Zn//M-V_2O_5NR/rGO and Stability tests over 2000 cycles of the aqueous ZIBs at a fixed current density of 4.0 A $g^{-1}$with the (Mn + Zn)-V_2O_5NR/rGO cathode [53], (b) Schematic diagram illustrating the mechanism of the pre-insertion strategy for restoring graphene oxide to expand the interlayer spacing to 2.00 nm and GCD cycling performance of GV at 2 A g^{-1} [54], (c) Working schematic diagram of the Zn//rGO/δ-NVO and long-term cycling performance at 2 A g^{-1} [55]

Sun et al. incorporated rGO into hydrated $V_2O_5 \cdot nH_2O$ (VOH) via APTES-mediated coupling, which widened the interlayer distance to 2.00 nm and permitted Zn^{2+} storage on both sides of the

DOI: 10.54254/2755-2721/2026.36832

sheets. The as-prepared V_2O_5/VG/CC cathode achieved 248 mAh g^{-1} at 2 A g^{-1}, sustained 83 % of its initial capacity after 5000 cycles, and maintained stable operation over 5000 cycles (Figure 3b) [54].

Tang and colleagues fabricated a flexible, freestanding paper-type electrode from rGO/δ-$Na_xV_2O_2 \cdot nH_2O$, CNTs, and cellulose fibers at a mass ratio of 5:4:1. This self-supporting sheet possessed a high areal loading of 5 mg cm^{-2}, a tensile strength of 8.51 MPa, and an electronic conductivity of 784.0 S m^{-1}. In electrochemical tests, it yielded 374.9 mAh g^{-1} at 0.1 A g^{-1} and still maintained 287.7 mAh g^{-1} at 2 A g^{-1}, while also displaying 92 % capacity retention over 4000 cycles. The overall charge storage was predominantly pseudocapacitive, with 80.3 % of the total contribution arising from capacitive effects (Figure 3c) [55].

4.1.3. Organic materials

Organic electrodes allow redox potential and active-site density to be tuned through molecular and functional-group design [56]. Carbonyl molecules such as benzoquinone can approach theoretical capacities of about 303 mAh g^{-1} through two-electron redox chemistry [57] and their conformational flexibility helps relieve volume change [58]. However, many organic electrodes have limited pi-electron delocalization and therefore low electronic conductivity [59, 60]. Low-molecular-weight organics may also dissolve into aqueous electrolytes, producing shuttle effects, active-material loss, and increased impedance at the zinc interface [61].

Geng et al. constructed an IDAQ/rGO cathode in which pi-pi interactions formed a mesoporous conductive network, overcoming the transport limitation of small organic molecules. As illustrated in Figure 4a, the electrode's activation arose from a phenol-to-quinone transformation, while the electrode itself delivered a capacity retention of 96 % over 5000 cycles at 2000 mA g^{-1}. Ex situ spectroscopy, GITT, and DFT results indicated a coupled Zn^{2+}/H^+ storage mechanism: Zn^{2+} supplied 79.4% of the capacity, H^+ contributed 20.6%, and the reaction was predominantly pseudocapacitive, with $IDAQ_2(H^+)_6(Zn^{2+})$ identified as the most stable discharged state [62]. The same group subsequently described a DNPT/rGO system (Pigment Blue 60). While rGO reduced the charge-transfer resistance from 28 to 4 Ω and tripled the electron-transfer rate constant, the cathode based on this composite delivered 120 mAh g^{-1} after 1000 cycles at 500 mA g^{-1} and 96 mAh g^{-1} at 20C, with carbonyl groups acting as the primary electrochemical active sites.(Figure 4b) DFT computations indicated $DNPT_2(H^+)_6(Zn^{2+})$ as the energetically preferred discharged species, consistent with the electrolyte's ionic distribution [63].

4.1.4. Prussian blue analogues

PBAs possess three-dimensional open frameworks with large channels, enabling fast Zn^{2+} diffusion and high-rate operation [64, 65]. Their compositions can avoid expensive or highly toxic elements, which benefits cost and environmental compatibility [64, 66]. Nevertheless, wet-chemical synthesis often generates $[M'(CN)_6]^{n-}$ vacancies and interstitial water [67]. These defects strengthen Zn^{2+} electrostatic interactions and increase diffusion barriers [68], while water in the framework accelerates electrolyte decomposition and structural distortion [67]. In mildly acidic media, hydrolysis of $[M'(CN)_6]^{n-}$ units may release HCN and continuously consume active material, making structural stability the central challenge for PBA cathodes.

DOI: 10.54254/2755-2721/2026.36832

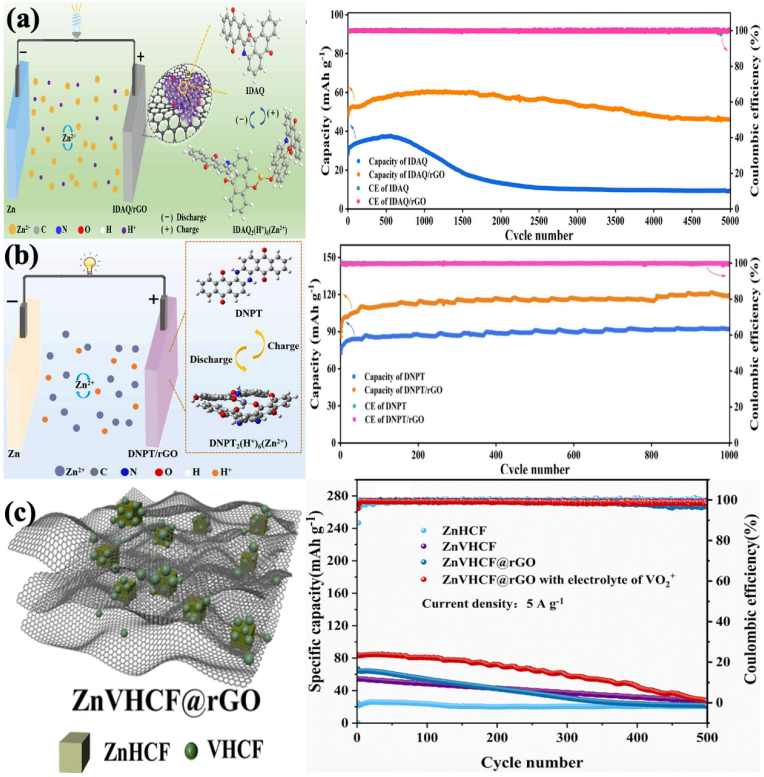

Figure 4. (a) Illustrated mechanism and diagram of IDAQ/rGO ZIBs using the IDAQ/rGO cathode and Zn anode in 3 M $Zn(CF_3SO_3)2$ electrolyte and IDAQ/rGO and IDAQ long cycling performance at 2000 mA g^{-1} [62]. (b) Working schematic diagram of the Zn//IDAQ/rGO and Long-term cycling stability and coulombic efficiency of DNPT/rGO and DNPT at 500 mA g^{-1} [63]. (c) Diagram of the cathode material and long-cycle performance under 5 A g^{-1} of materials [69]

Addressing the persistent issues of PBAs—insufficient capacity, poor conductivity, and vanadium dissolution—Hu and colleagues integrated two modifications: in-situ growth of ZnVHCF@rGO on rGO, and addition of 0.1 M VO_2^+ to the electrolyte (based on sol-equilibrium principles). The combined effect of V/Fe dual-metal sites and the rGO conductive skeleton afforded a capacity of 152.3 mAh g^{-1} at 0.1 A g^{-1}. After VO_2^+ was introduced, this value climbed to 166.8 mAh g^{-1}, benefiting from the extra vanadium redox activity as well as the suppressed dissolution behavior. Ex-situ XRD and XPS confirmed reversible Zn^{2+} (de)intercalation, a cubic-to-rhombohedral structural evolution of VHCF, and concomitant valence variations of V and Fe. At 5 A g^{-1}, the 300-cycle capacity retention jumped from 46.9% to 72.1%, with near-unity Coulombic efficiency (Figure 4c); kinetic measurements disclosed a 90.24% capacitive fraction at 1 mV s^{-1} and diffusion coefficients of 10^{-7}–10^{-10} cm^2 s^{-1} [69].

4.2. Anode

Figure 5 summarizes four main roles of graphene-based architectures in aqueous zinc anodes: artificial interfacial protection, three-dimensional conductive hosts, intercalation-type zinc-free anodes, and metal-free capacitive electrodes. These roles arise from graphene's two-dimensional lamellar morphology, high conductivity, large surface area, and chemical resistance.

(1) Artificial Interfacial Protection Layers

(2) Three-Dimensional Conductive Host Scaffolds

DOI: 10.54254/2755-2721/2026.36832

(3) Intercalation-Type Anode Candidates
(4) Metal-Free Capacitive Electrodes

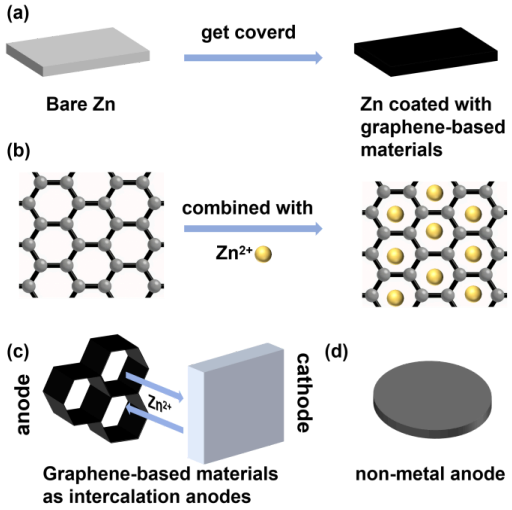

Figure 5. Several application forms of graphene-based materials in the negative electrode. (a) Artificial interfacial protection layers, (b) three-dimensional conductive host scaffolds, (c) intercalation-type anode candidates, (d) metal-free capacitive electrodes

Zhu et al. spray-coated a nitrogen-deficient graphitic carbon nitride (NDCN) interlayer on zinc anodes. The layer reduced the Zn^{2+} nucleation overpotential from 116.2 to 43.1 mV, promoted preferential (002) deposition by increasing the relative intensity ratio from 0.39 to 1.7, and lowered hydrogen-evolution/corrosion currents to 68.7% of those measured on bare zinc. Symmetric cells operated for more than 2000 h at 5 mA cm^{-2} with only 16.7 mV hysteresis. In MnO_2||NDCN@Zn full cells, about 88% of the initial capacity remained after 2300 cycles at 1 A g^{-1}, with 98.6% Coulombic efficiency.(Figure 6a) DFT calculations attributed the improvement partly to weaker water adsorption on the modified surface [70].

Lin and co-workers developed a binder-free 3D Zn–graphene (Zn–G) anode through a self-sustaining reaction between Zn powder and GO. The incorporated graphene skeleton played a dual role: it suppressed zinc dendrites and reduced undesired interfacial reactions. In symmetric cell tests, this electrode operated stably for more than 550 h at 1 mA cm^{-2}/1 mAh cm^{-2} and 180 h at 15 % DOD. Furthermore, a full cell combining this anode with a MnO_2@CNT cathode survived over 1600 cycles at 0.5 A g^{-1}, maintained 74.5 % capacity at the 1000-cycle mark (N/P = 3), and provided an energy density of 30–70 Wh kg^{-1}(Figure 6b) [71].

A metal-free full cell composed of a $ZnMn_2O_4$/CB cathode and a h-WO_3/3DG anode (the latter being a Zn-free material from Chen's group) offered 73.5 Wh kg^{-1} and retained 76.6 % of its original capacity following 1000 cycles. The anode itself possessed large hexagonal tunnels of about 5.36 Å and a hydrophilic, high-surface-area graphene scaffold (757.9 m^2 g^{-1}), which enhanced Zn^{2+} mobility with diffusivity values in the range of $10^{-9.5}$–$10^{-12.8}$ cm^2 s^{-1}. Separately, this electrode in a half-cell delivered 115.6 mAh g^{-1} at 0.1 A g^{-1} and preserved roughly 89 % capacity after 10 000 cycles at 2 A g^{-1}(Figure 6c) [72].

DOI: 10.54254/2755-2721/2026.36832

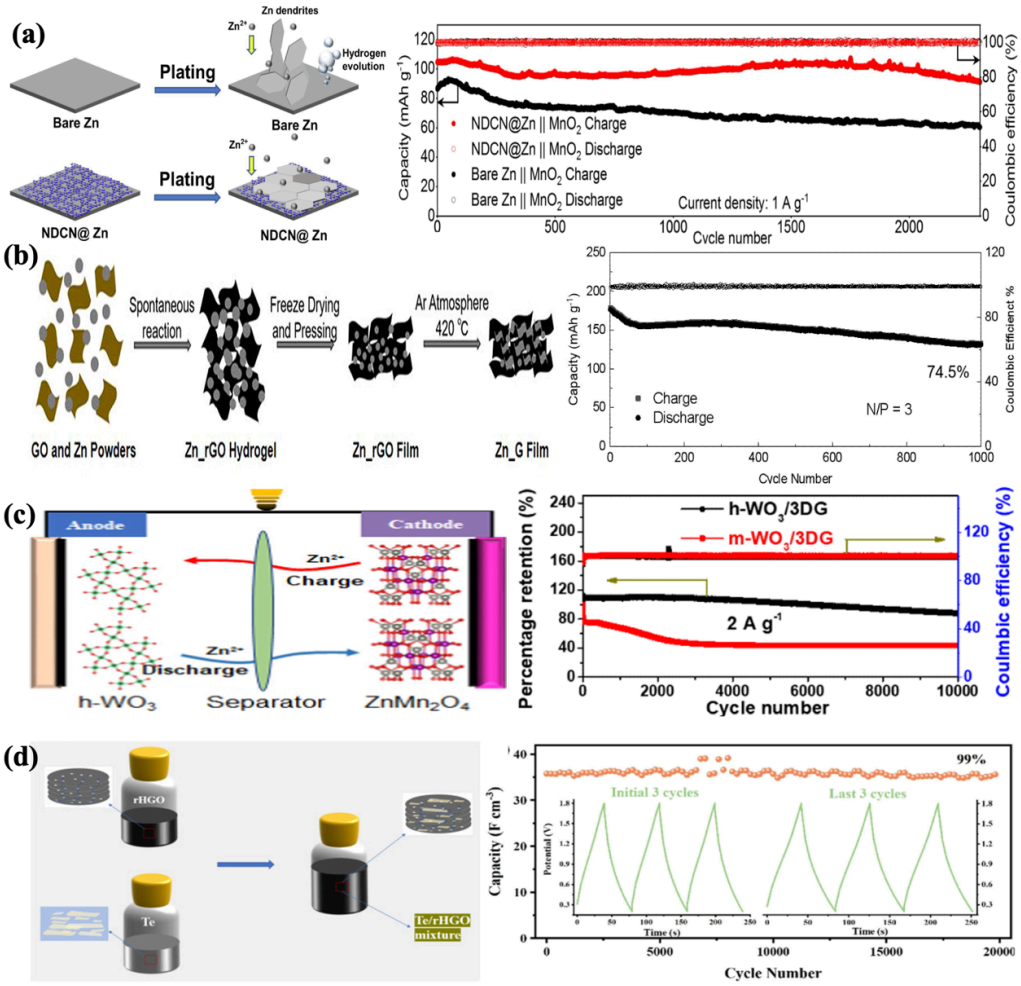

Figure 6. (a) Schematic diagram of NDCN coating on commercial zinc foil surface and Long-term cycling performance of the full cells tested at 1 A g^{-1} [70], (b) Schematic diagram of the Zn_G preparation process and the calculated energy densities of the Zn//MnO_2 with Zn_G and Zn_F as anodes under different N/P ratios [71]. (c) Working schematic diagram of the $ZnMn_2O_4$//h-WO_3 and cycling stability at 2.0 A g^{-1} [72]. (d) Preparation process of Te/rHGO thin film and Long-cycling capability of this ZIC device under the current density of 4 mA cm^{-2}, the inset image reveals the initial 3 cycles and the last 3 cycles of GCD curves [73]

Chen et al. further developed a sandwich-like Te/rHGO conversion anode for flexible ZIBs and zinc-ion hybrid capacitors. Te nanoribbons store Zn^{2+} through the Te to $ZnTe_2$ to ZnTe conversion sequence, while rHGO provides conductivity, flexibility, and space for volume change. A ZIB using an rHGO/$ZnMnO_2$ cathode delivered 197.23 mAh cm^{-3}, 387.1 mWh cm^{-3}, and 93.3% capacity retention after 3500 cycles. A zinc-ion hybrid capacitor reached 75.87 F cm^{-3} and retained its capacitance over 20,000 cycles. The electrode also showed a higher hydrogen-evolution overpotential than zinc foil and stable CV behavior under bending from 0 to 180 degrees (Figure 6d) [73].

DOI: 10.54254/2755-2721/2026.36832

4.3. Electrolytes

GBs can function in electrolytes either as dispersed liquid additives or as components of hydrogel networks. Oxygen-containing groups on graphene derivatives help redistribute Zn^{2+} flux and suppress dendrite formation; small additions of GO, typically 0.5-2 wt%, can markedly extend cycle life. In hydrogel electrolytes, graphene-based frameworks form bicontinuous structures with polymers, combining ionic conduction, electronic pathways, and water affinity, while controlled hydrophobic domains can reduce hydrogen evolution.

Lee et al. added 2-4 nm oxygen-rich GO quantum dots (GOQDs) to aqueous ZIB electrolytes. The GOQDs adjusted Zn^{2+} solvation, suppressed dendrites and H_2 evolution, and generated a Zn-C/O-bonded interfacial layer that stabilized the Zn(100) facet. As a result, Zn||Zn symmetric cells cycled for 150 h, about three times longer than the control, and $Na_2V_6O_{16.2}H_2O$||Zn full cells retained 81.0% capacity after 3000 cycles at 1 A g^{-1}(Figure 7a) [74].

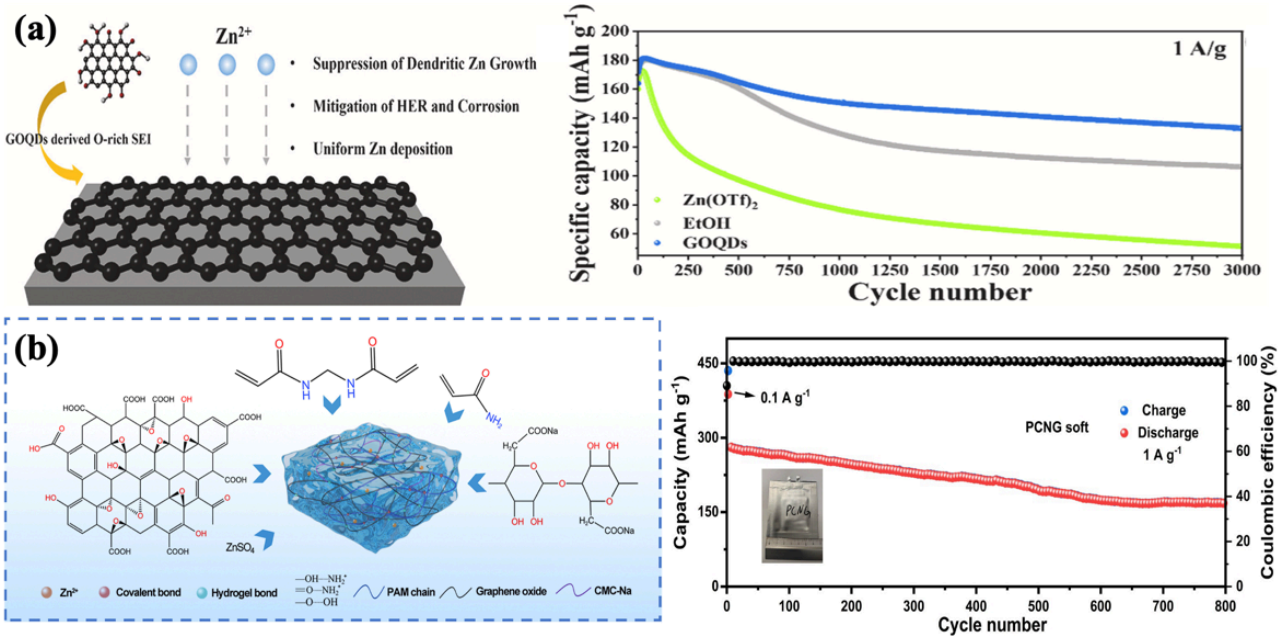

Figure 7. (a) The mechanism of GOQDs action and Long-term cycling stability at 1 A g^{-1}, showing enhanced capacity retention upon GOQDs incorporation [74]. (b) The schematic illustration of the synthesis of PCNG hydrogel electrolyte and cycling stability at 1.0 A g^{-1} [75]

A hydrogel electrolyte composed of polyacrylamide, sodium carboxymethylcellulose, and GO (termed PCNG) was designed by Liu et al. The resulting full cell pairing a graphene/sodium vanadate cathode with this electrolyte delivered 167.8 mAh g^{-1} after 800 cycles at 1.0 A g^{-1} (Figure 7b) and continued to operate under bending or folding conditions. Symmetric Zn||Zn cells also benefited from this electrolyte, achieving 1000 h of stable cycling at 0.2 mA cm^{-2} with a corrosion current of 0.053 mA cm^{-2}. These electrochemical improvements originate from the PCNG's multiple hydrogen-bond network, which restricts free water mobility to curtail H_2 evolution and dendrite formation, alongside its favorable physicochemical properties: ionic conductivity of 45.5 mS cm^{-1}, an extended voltage window up to 2.5 V, and 200% stretchability. Moreover, the oxygen groups in PCNG contribute to uniform Zn(002)-oriented deposition via electrostatic shielding and current redistribution, thus minimizing the detrimental tip effect [75].

DOI: 10.54254/2755-2721/2026.36832

4.4. Separators

Glass-fiber separators have high porosity, but their broad pore-size distribution and low modulus make them ineffective barriers against zinc dendrites. GO or rGO modification, either as a coating or as a composite phase, can introduce nanoscale interlayer channels and high in-plane strength. Oxygen-rich groups further anchor Zn^{2+}, homogenize ion flux, and promote more uniform nucleation.

Utilizing the zincophilic nature of GO–TiO_2 (adsorption energy: –0.567 eV), Chen et al. constructed a Janus separator comprising a polyamide/GO–TiO_2 nanofiber layer electrospun on a commercial glass fiber support. This separator exhibited a notable ionic conductivity of 16.1 mS cm^{-1} and a Zn^{2+} transference number of 0.82. In symmetric cells, it offered exceptional longevity—over 2000 h at 1 mA cm^{-2}, >1800 h at 2 mA cm^{-2}, and >600 h at 5 mA cm^{-2}—compared with the pristine glass fiber separator. Meanwhile, in full cells with MnO_2 cathodes, it gave an initial capacity of 112.1 mAh g^{-1} and a retention of 60.57 % after 500 cycles (Figure 8a). The underlying mechanism, as revealed by DFT, SEM, and XRD, is that the GO–TiO_2 species effectively steer Zn(002) plane deposition and reduce dendritic and parasitic issues, corroborating its robust zinc affinity [76]. Zhang et al. reported an ultrathin 12 um MCNF separator made from a cellulose nanofiber membrane functionalized with a Cu/graphene interfacial layer. The hydroxyl-rich nanoporous cellulose scaffold and zincophilic conductive Cu/graphene layer homogenized Zn^{2+} flux, increased the transference number to 0.78, accelerated desolvation and nucleation, and reduced corrosion. With MCNF, Zn||Zn cells operated for 700 h and 340 h at 5 and 10 mA cm^{-2}, respectively. Under lean electrolyte conditions of 25 uL cm^{-2}, Zn||VO_2 full cells cycled for more than 1800 cycles (Figure 8b), highlighting the value of thin separators for high-energy-density aqueous ZIBs [77].

4.5. Current collectors

Current collectors provide mechanical support and electrical pathways, but their surface chemistry also controls zinc nucleation and growth. An effective collector should combine high conductivity, electrochemical stability, zincophilicity, and mechanical compliance. Conventional metal foils such as Cu, Ti, and stainless steel conduct electrons well, yet they are susceptible to corrosion, hydrogen evolution, and dendrite-induced short circuits, which lowers efficiency and cycle life. Graphene-based coatings, frameworks, or interlayers can redistribute current density, guide compact nucleation, buffer volume change, suppress parasitic reactions, and in some designs serve as metal-free collectors. This section reviews recent progress in graphene-modified current collectors for ZIBs.

Heo et al. sequentially deposited graphene and CNT layers on stainless steel foil and then annealed the structure at 400 deg C, producing a CNT@G-SSF current collector with improved conductivity, wettability, and adhesion. The coating removed surface oxides and decreased interfacial charge-transfer resistance from 197.95 to 78.25 ohm, while the porous CNT layer reduced the electrolyte contact angle from 77 deg to 18 deg. A ZIB using this cathode collector delivered 236.8 mAh g^{-1} at 0.3C and 127.6 mAh g^{-1} at 2.0C, and retained 99.0% capacity after 1000 cycles at 1.0C.(Figure 8c) These values exceeded those of unmodified SSF (70.3 mAh g^{-1}) and G-SSF (208.2 mAh g^{-1}). At a mass loading of about 13.0 mg, the electrode delivered 2.04 mAh cm^{-2} and inhibited dendrite formation [21].

DOI: 10.54254/2755-2721/2026.36832

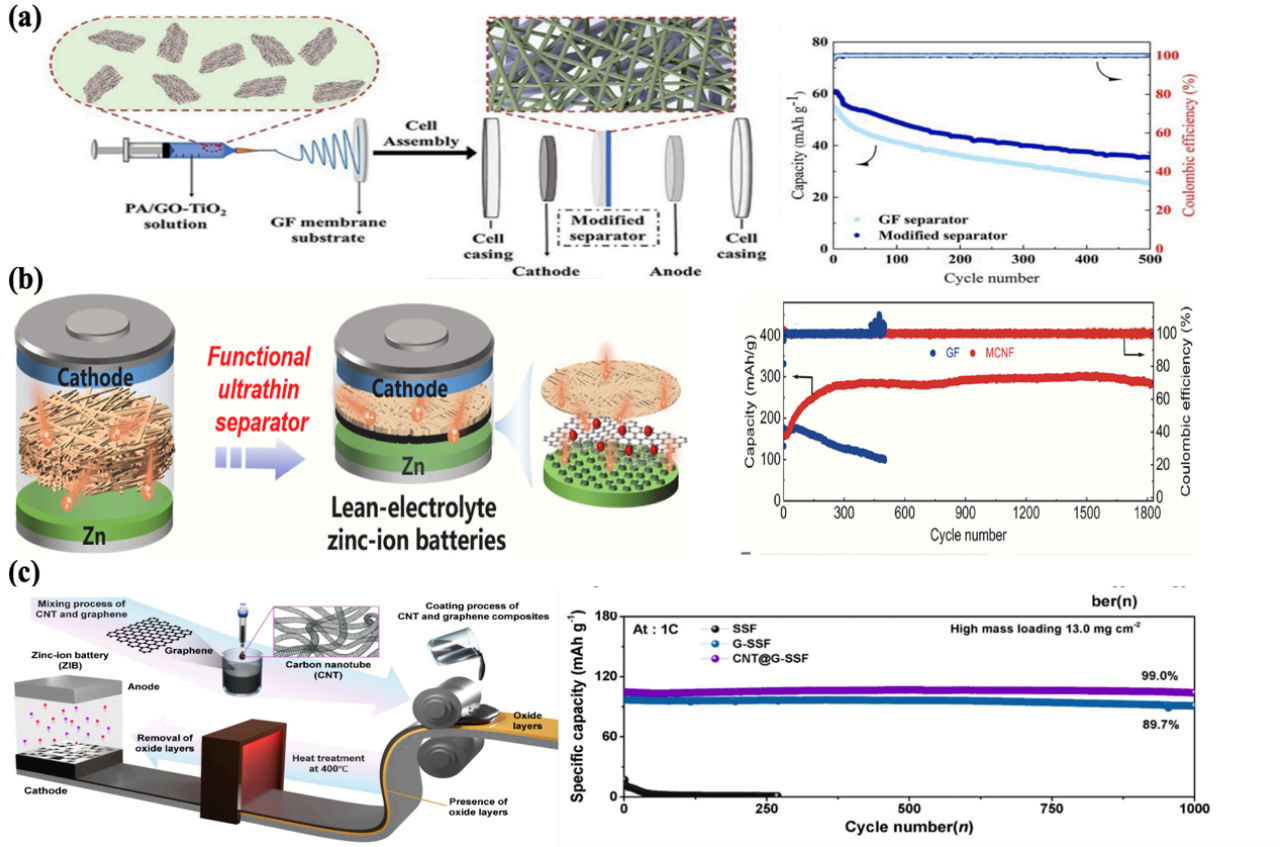

Figure 8. (a) Schematic fabrication process of modified separator and Long-term cycling performance of Zn//MnO_2 full cells using different separators at 5C for 500 cycles [76]. (b) Diagram of the diaphragm and cycling performance at 2 A/g [77]. (c) Fabrication of proposed CNT@G-SSF cathode current collector for ZIBs and Cycling stability of ZIBs with high mass loading [21]

5. Conclusion

GBs have substantially improved the performance of aqueous ZIBs, but unresolved challenges remain in each battery component.

Cathode outlook: Graphene/active-material interfaces are frequently dominated by physical contact rather than robust chemical bonding, so conductive pathways may break during long cycling. Ion insertion also remains difficult to control at the molecular level; nonuniform intercalation can drive agglomeration and block transport channels. Graphene alone cannot fully eliminate side reactions such as Mn^{3+} disproportionation, irreversible V^{5+} reduction, or structural rearrangement in organic electrodes. In addition, graphene loading must be balanced against conductivity, capacity, flexibility, and practical areal capacity, especially when mass loading exceeds 10 mg cm^{-2}.

Anode outlook: Graphene-rich protective layers may crack, peel, or locally detach during deep plating/stripping, increasing interfacial impedance. Zincophilic N, O, or S functional groups can gradually lose activity, leading to uneven Zn^{2+} distribution and renewed dendrite growth. Hydrogen evolution is reduced but not completely removed, and high-surface-area three-dimensional hosts may even intensify it, lowering Coulombic efficiency. More systematic optimization of coating

DOI: 10.54254/2755-2721/2026.36832

thickness, porosity, and wetting properties is needed, together with simpler and cheaper synthesis methods.

Electrolyte outlook: GOQD additives and three-dimensional hydrogel networks can improve interfacial regulation, yet many full cells at high rates still retain only about 80% capacity after thousands of cycles, and symmetric-cell lifetimes often remain below 1000 h. Hydrogel systems also face a flexibility-conductivity compromise, with typical ionic conductivities of 27-45 mS cm^{-1}, and repeated deformation can increase contact resistance. Low-temperature operation is especially weak; capacity retention at -20 deg C is rarely above 22%. During long cycling, graphene fillers may agglomerate or migrate, weakening ion-flux regulation and hydrogen-evolution suppression.

Separator outlook: Graphene-based separators often rely on high-temperature reduction, sacrificial templates, or complicated liquid-phase processing, which raises cost and limits scalability. Functional layers may exfoliate, aggregate, or collapse during extended electrochemical operation. Precise control over the density and chemical identity of surface groups is also difficult, restricting Zn^{2+} flux homogenization. Under lean-electrolyte conditions, parasitic products accumulate more rapidly and ion transport becomes more constrained.

Current-collector outlook: Oxides trapped between graphene coatings and metal substrates can maintain residual contact resistance. Defects introduced during fabrication, including oxygen groups and vacancies, reduce intrinsic conductivity. At mass loadings above 10 mg cm^{-2}, planar two-dimensional collectors may create uneven electron distribution and local current-density hot spots. Graphene's hydrophobicity also limits electrolyte wetting; even after hydrophilic modification, local drying or by-product accumulation can degrade interfacial contact during long cycling.

Future research should shift from isolated material demonstrations to integrated cell-level engineering. Priority directions include strengthening chemical bonding at graphene/active-material interfaces, passivating defects that reduce conductivity or trigger parasitic reactions, developing scalable graphene architectures with controlled porosity, thickness, and functionalization, and clarifying dynamic failure mechanisms through in situ characterization and modeling. Progress on these issues will determine whether GBs can move from laboratory performance enhancement to reliable components in practical aqueous ZIBs.

References

[1] Zhou, D., Pye, S., Verrier, B., et al. (2026). The implications of uncertainties on global lithium resources availability estimations. *Iscience, 29*(2).

[2] Wang, Q., Mao, B., Stoliarov, S., et al. (2019). A review of lithium ion battery failure mechanisms and fire prevention strategies. *Progress in Energy and Combustion Science, 73*, 95–131.

[3] Yang, X., Zhang, H., Liu, Q., et al. (2025). The Li-ion battery industry and its challenges. *Nature Reviews Chemistry, 9*(8), 497–8.

[4] Innocenti, A., Bresser, D., Garche, J., et al. (2024). A critical discussion of the current availability of lithium and zinc for use in batteries. *Nature Communications, 15*(1).

[5] Liu, S., Zhang, R., Wang, C., et al. (2024). Zinc ion batteries: Bridging the gap from academia to industry for grid-scale energy storage. *Angewandte Chemie-International Edition, 63*(17).

[6] Shiam, S., Rath, J., Kiani, A. (2024). Advances in transition metal oxide cathodes for zinc-ion batteries - A review focusing on safety and toxicity. *International Journal of Electrochemical Science, 19*(11).

[7] Jia, X., Ye, J., Zheng, Y., et al. (2026). Manganese ions induced pillaring and interplanar engineering of ultra-thin $NH_4V_4O_{10}$ nanobelts toward efficient zinc-ion storage. *Journal of Power Sources, 671*.

[8] Zhao, Y., Shen, Y., Zhang, Y., et al. (2025). Key issues in surface and interface of Zn anode and interfacial manipulation strategies toward high performance Zn-ion batteries. *Materials Today Energy, 53*.

[9] Zhang, S., Zhang, J., & Ha, S. (2025). Mechanistic insight into the effect of zinc anode roughness on V_2O_5 cathode degradation in aqueous Zn-ion batteries. *Materials Letters, 399*.

DOI: 10.54254/2755-2721/2026.36832

[10] Yang, K., Hu, Y., Zhang, T., et al. (2022). Triple-functional polyoxovanadate cluster in regulating cathode, anode, and electrolyte for tough aqueous zinc-ion battery. *Advanced Energy Materials, 12*(42).
[11] Zhu, J., Bie, Z., Cai, X., et al. (2022). A molecular-sieve electrolyte membrane enables separator-free zinc batteries with ultralong cycle life. *Advanced Materials, 34*(43).
[12] Li, L., Yue, S., Jia, S., et al. (2024). Recent advances in graphene-based materials for zinc-ion batteries. *Chemical Record, 24*(4).
[13] Novoselov, K., Geim, A., Morozov, S., et al. (2004). Electric field effect in atomically thin carbon films. *Science, 306*(5696), 666–669.
[14] Emon, S., Hossain, M., Khanam, M., et al. (2025). Expanding horizons: Taking advantage of graphene's surface area for advanced applications. *Applied Sciences-Basel, 15*(8).
[15] Wang, C., Wang, M., He, Z., et al. (2020). Rechargeable aqueous zinc-manganese dioxide/graphene batteries with high rate capability and large capacity. *Acs Applied Energy Materials, 3*(2), 1742–1748.
[16] Sun, Y., Papageorgiou, D., Humphreys, C., et al. (2021). Mechanical properties of graphene. *Applied Physics Reviews, 8*(2).
[17] Chen, X., Sun, B., Li, Q., et al. (2024). Synergistic effect of Sn doped manganese oxide and conductive reduced graphene oxide for zinc ion battery. *Journal of Power Sources, 622*.
[18] Zhang, N., Chen, X., Yu, M., et al. (2020). Materials chemistry for rechargeable zinc-ion batteries. *Chemical Society Reviews, 49*(13), 4203–4219.
[19] Wu, B., Mu, Y., Li, Z., et al. (2023). Realizing high-voltage aqueous zinc-ion batteries with expanded electrolyte electrochemical stability window. *Chinese Chemical Letters, 34*(2).
[20] Wu, H., Gao, S., Pang, Y., et al. (2025). Stabilizing aqueous zinc-ion battery with cellulose/graphene hybrid separator through dual regulation of fast desolvation and ion deposition. *Journal of Power Sources, 650*.
[21] Heo, H., Lee, J., Jo, Y., et al. (2025). Synergistic enhancement of Zn-ion battery performance using CNT/graphene composite-coated stainless-steel-foil current collectors. *Composite Structures, 372*.
[22] Wu, Z., Xu, C., Zeng, J., et al. (2025). A review of 3D graphene materials for energy storage and conversion. *New Carbon Materials, 40*(3), 477–517.
[23] Bertaglia, T., Neubert, T., Iost, R., et al. (2025). Consequences of edge and substrate modifications on graphene electrochemistry. *Current Opinion in Electrochemistry, 50*.
[24] Mu, Y., Li, Z., Wu, B., et al. (2023). 3D hierarchical graphene matrices enable stable Zn anodes for aqueous Zn batteries. *Nature Communications, 14*(1).
[25] Pei, Y., Liu, Y., Kong, C., et al. (2026). Graphene-based composites as the cathodes for high-performance aqueous zinc-ion batteries: Applications and perspectives. *Chinese Chemical Letters, 37*(4).
[26] Leitherer, S., Coto, P., Ullmann, K., et al. (2017). Charge transport in C_{60}-based single-molecule junctions with graphene electrodes. *Nanoscale, 9*(21), 7217–26.
[27] Bi, S., Wang, H., Wang, R., et al. (2022). Two-dimensional materials for aqueous zinc-ion batteries. *2D Materials, 9*(4).
[28] Liu, J., Qin, H., Liu, Y. (2021). Multi-scale structure-mechanical property relations of graphene-based layer materials. *Materials, 14*(16).
[29] Li, Y., Wu, L., Dong, C., et al. (2023). Manipulating horizontal Zn deposition with graphene interpenetrated Zn hybrid foils for dendrite-free aqueous zinc ion batteries. *Energy & Environmental Materials, 6*(5).
[30] Fasehullah, M., Jamil, S., Ali, G., et al. (2025). Surface engineering of single-crystal NCM811 with graphene for enhanced mechanical integrity. *Chemical Engineering Journal, 524*.
[31] Li, H., Ma, L., Han, C., et al. (2019). Advanced rechargeable zinc-based batteries: Recent progress and future perspectives. *Nano Energy, 62*, 550–87.
[32] Shen, C., Li, X., Li, N., et al. (2018). Graphene-boosted, high-performance aqueous Zn-ion battery. *ACS Applied Materials & Interfaces, 10*(30), 25446–53.
[33] Wang, F., Borodin, O., Gao, T., et al. (2018). Highly reversible zinc metal anode for aqueous batteries. *Nature Materials, 17*(6), 543–+.
[34] Kundu, D., Adams, B., Duffort, V., et al. (2016). A high-capacity and long-life aqueous rechargeable zinc battery using a metal oxide intercalation cathode. *Nature Energy, 1*.
[35] Zhang, N., Cheng, F., Liu, Y., et al. (2016). Cation-deficient spinel $ZnMn_2O_4$ cathode in $Zn(CF_3SO_3)_2$ electrolyte for rechargeable aqueous Zn-ion battery. *Journal of the American Chemical Society, 138*(39), 12894–901.
[36] Xu, C., Li, B., Du, H., et al. (2012). Energetic zinc ion chemistry: The rechargeable zinc ion battery. *Angewandte Chemie-International Edition, 51*(4), 933–5.
[37] Pan, H., Shao, Y., Yan, P., et al. (2016). Reversible aqueous zinc/manganese oxide energy storage from conversion reactions. *Nature Energy, 1*.

DOI: 10.54254/2755-2721/2026.36832

[38] Alfaruqi, M., Mathew, V., Gim, J., et al. (2015). Electrochemically induced structural transformation in a γ-MnO_2 cathode of a high capacity zinc-ion battery system. *Chemistry of Materials, 27*(10), 3609–20.
[39] Sun, W., Wang, F., Hou, S., et al. (2017). Zn/MnO_2 battery chemistry with H^+ and Zn^{2+} coinsertion. *Journal of the American Chemical Society, 139*(29), 9775–8.
[40] Huang, J., Wang, Z., Hou, M., et al. (2018). Polyaniline-intercalated manganese dioxide nanolayers as a high-performance cathode material for an aqueous zinc-ion battery. *Nature Communications, 9*.
[41] Li, Y., Zhang, Y., Gan, Z., et al. (2026). Microwave-hydrothermal graphene synergy boosts α-MnO_2 cathode for high-performance Zn-ion batteries. *Materials Research Bulletin, 196*.
[42] Ding, S., Zhang, M., Qin, R., et al. (2021). Oxygen-deficient β-MnO_2@graphene oxide cathode for high-rate and long-life aqueous zinc ion batteries. *Nano-Micro Letters, 13*(1).
[43] Wang, C., Zeng, Y., Xiao, X., et al. (2020). γ-MnO_2 nanorods/graphene composite as efficient cathode for advanced rechargeable aqueous zinc-ion battery. *Journal of Energy Chemistry, 43*, 182–187.
[44] Yang, S., Chen, Z., Fu, P., et al. (2026). Mild production of Mn_3O_4-reduced graphene oxide cathode for aqueous zinc-ion batteries with outstanding performance. *Journal of Power Sources, 663*.
[45] Zeng, J., Zhang, Z., Guo, X., et al. (2019). A conjugated polyaniline and water co-intercalation strategy boosting zinc-ion storage performances for rose-like vanadium oxide architectures. *Journal of Materials Chemistry A, 7*(37), 21079–21084.
[46] Cao, W., Zou, Z., Liang, F., et al. (2025). Research progress on vanadium oxides as cathode materials for aqueous zinc-ion batteries: Review. *Journal of Materials Science-Materials in Electronics, 36*(25).
[47] Fan, L., Ru, Y., Xue, H., et al. (2020). Vanadium-based materials as positive electrode for aqueous zinc-ion batteries. *Advanced Sustainable Systems, 4*(12).
[48] Cao, J., Zhang, D., Yue, Y., et al. (2022). Boosting Zn^{2+} diffusion via tunnel-type hydrogen vanadium bronze for high-performance zinc ion batteries. *Acs Applied Materials & Interfaces, 14*(6), 7909–7916.
[49] Wang, S., Ma, C., Ding, J., et al. (2026). Tunnel-preinserted guest zinc tailoring VO_2(B) enhances Zn^{2+}/H^+ reversible de/intercalation capability. *Advanced Functional Materials, 36*(14).
[50] Li, W., Jiang, W., Zhu, K., et al. (2024). Unlocking the performance degradation of vanadium-based cathodes in aqueous zinc-ion batteries. *Chemical Engineering Journal, 496*.
[51] Guo, J., Ma, W., Zheng, Y., et al. (2023). Cation pre-intercalation and oxygen vacancies in vanadium oxide for synergistically enhanced high-rate and stability for zinc-ion batteries. *Applied Surface Science, 612*.
[52] Song, T., Fan, W., Hu, Y., et al. (2025). Advances and future perspectives of composite strategies in vanadium-/manganese-based cathode materials for aqueous zinc-ion batteries. *Green Chemistry, 27*(34), 10071–93.
[53] Muthukumar, K., Rajendran, S., Sekar, A., et al. (2023). Synthesis of V_2O_5 nanoribbon-reduced graphene oxide hybrids as stable aqueous zinc-ion battery cathodes via divalent transition metal cation-mediated coprecipitation. *Acs Sustainable Chemistry & Engineering, 11*(6).
[54] Sun, J., Yang, J., Zhang, Y., et al. (2025). Reduced graphene oxide pre-intercalation enables double-sided Zn^{2+} storage between VO layers in V_2O_5•nH_2O. *Energy Storage Materials, 83*.
[55] Tang, F., Zhou, W., Chen, M., et al. (2019). Flexible free-standing paper electrodes based on reduced graphene oxide/δ-$Na_xV_2O_5$•nH_2O nanocomposite for high-performance aqueous zinc-ion batteries. *Electrochimica Acta, 328*.
[56] Hong, Y., Ma, Z., Li, K., et al. (2023). Research progress and perspectives on ultra-low temperature organic batteries. *Journal of Materials Chemistry A, 11*(15), 7898–923.
[57] Lin, Z., Shi, H., Lin, L., et al. (2021). A high capacity small molecule quinone cathode for rechargeable aqueous zinc-organic batteries. *Nature Communications, 12*(1).
[58] Gong, S., Chao, Y., Yang, F., et al. (2024). Bifunctional potential structure design breaks electrolyte limitations of zinc ion battery. *Angewandte Chemie-International Edition, 63*(18).
[59] Heiska, J., Nisula, M., Karppinen, M. (2019). Organic electrode materials with solid-state battery technology. *Journal of Materials Chemistry A, 7*(32), 18735–58.
[60] Lu, Y., Chen, J. (2020). Prospects of organic electrode materials for practical lithium batteries. *Nature Reviews Chemistry, 4*(3), 127–42.
[61] Lau, V., Moudrakovski, I., Yang, J., et al. (2020). Uncovering the shuttle effect in organic batteries and counter-strategies thereof: A case study of the N, N′-dimethylphenazine cathode. *Angewandte Chemie-International Edition, 59*(10), 4023–34.
[62] Geng, X., Jiang, Y., Ma, H., et al. (2022). Long-life aqueous zinc-ion batteries of organic iminodianthraquinone/rGO cathode assisted by Zn^{2+} binding with adjacent molecules. *Acs Applied Materials & Interfaces, 14*(44), 49746–54.
[63] Geng, X., Ma, H., Lv, F., et al. (2022). Ultrastable organic cathode derived by pigment/rGO for aqueous zinc-ion batteries. *Chemical Engineering Journal, 446*.

DOI: 10.54254/2755-2721/2026.36832

[64] Wang, J., Hu, Z., Qi, Y., et al. (2025). Prussian blue analogues for aqueous zinc-ion batteries: Recent process and perspectives. *Journal of Materials Science & Technology, 221*, 302–20.
[65] Wang, M., Ma, J., Lu, K., et al. (2024). Continuous and scalable synthesis of Prussian blue analogues with tunable structure and composition in surfactant-free microreactor for stable zinc-ion storage. *Chemsuschem, 17*(18).
[66] Xu, C., Yang, Z., Zhang, X., et al. (2021). Prussian blue analogues in aqueous batteries and desalination batteries. *Nano-Micro Letters, 13*(1).
[67] Zhao, L., Zhao, Y., Wu, Y., et al. (2025). Everything in aqueous zinc-ion batteries may be Prussian blue analogues: From cathode materials to electrolyte additives applications. *Energy Storage Materials, 78*.
[68] Wang, L., Liu, N., Li, Q., et al. (2025). Dual redox reactions of silver hexacyanoferrate Prussian blue analogue enable superior electrochemical performance for zinc-ion storage. *Angewandte Chemie-International Edition, 64*(4).
[69] Hu, B., Li, D., Li, M., et al. (2025). Conductive network enhanced self-assembled diphasic Prussian blue analogs for aqueous zinc-ion batteries. *Journal of Materials Chemistry C, 13*(13), 6736–44.
[70] Zhu, D., Li, J., Ren, F., et al. (2023). Towards a high-performance anode for zinc metal batteries: A tri-functional nitrogen-defective graphitic carbon nitride material for anode protection. *Journal of Colloid and Interface Science, 651*, 504–13.
[71] Lin, Y., Hu, Y., Zhang, S., et al. (2022). Binder-free freestanding 3D Zn-graphene anode induced from commercial zinc powders and graphene oxide for zinc ion battery with high utilization rate. *Acs Applied Energy Materials, 5*(12), 15222–32.
[72] Chen, X., Huang, R., Ding, M., et al. (2022). Hexagonal WO_3/3D porous graphene as a novel zinc intercalation anode for aqueous zinc-ion batteries. *Acs Applied Materials & Interfaces, 14*(3), 3961–9.
[73] Chen, Q., Wang, L., Chen, X., et al. (2025). Sandwich-like tellurium nanoribbons/graphene composited film as conversion-type non-metal anode for flexible Zn-ion electrochemical energy storage devices. *Surfaces and Interfaces, 56*.
[74] Lee, J., Park, Y., Lee, K., et al. (2026). Graphene oxide quantum dots as an additive in the electrolyte for enhanced cycle retention of zinc-ion secondary battery. *Carbon, 249*.
[75] Liu, Y., Zhang, X., Jia, C., et al. (2025). Graphene enhanced hydrogel electrolyte boost flexible zinc ion battery stability. *Electrochimica Acta, 538*.
[76] Chen, Y., Gao, C., Li, J., et al. (2024). Organic/inorganic functional Janus separator for high-performance zinc anode. *Journal of Energy Storage, 103*.
[77] Zhang, K., Xie, S., Liang, J., et al. (2025). Functional ultrathin separators enabling stable zinc anodes for lean-electrolyte zinc-ion batteries. *Journal of Membrane Science, 722*.